Near-infrared metamaterials with dual-band negative-index characteristics

Do-Hoon Kwon and Douglas H. Werner

Department of Electrical Engineering, The Pennsylvania State University
University Park, PA 16802, USA

dhw@psu.edu

Alexander V. Kildishev and Vladimir M. Shalaev

Birck Nanotechnology Center, School of Electrical and Computer Engineering
Purdue University, West Lafayette, IN 47907, USA

Abstract: Dual-band negative-index metamaterial designs in the near-infrared frequency range are presented and their performance is analyzed using a full-wave numerical electromagnetic scattering method. Negative effective permittivity is provided by a thin layer of metallic film. Negative effective permeabilities are supplied in two distinct frequency bands by magnetic resonators of different dimensions.

OCIS codes: (160.4760) Materials (310.6860) Thin films

References and links

1. R. A. Shelby, D. R. Smith, and S. Schultz, "Experimental verification of a negative index of refraction," Science **292**, 77–79 (2001).
2. J. B. Pendry, "Negative refraction makes a perfect lens," Phys. Rev. Lett. **85**, 3966–3969 (2000).
3. S. Zhang, W. Fan, N. C. Panoiu, K. J. Malloy, R. M. Osgood, and S. R. J. Brueck, "Experimental demonstration of near-infrared negative-index metamaterials," Phys. Rev. Lett. **95**, 137404 (2005).
4. S. Zhang, W. Fan, K. J. Malloy, S. R. J. Brueck, N. C. Panoiu, and R. M. Osgood, "Near-infrared double negative metamaterials," Opt. Express **13**, 4922–4930 (2005).
5. V. M. Shalaev, W. Cai, U. K. Chettiar, H.-K. Yuan, A. K. Sarychev, V. P. Drachev, and A. V. Kildishev, "Negative index of refraction in optical metamaterials," Opt. Lett. **30**, 3356–3358 (2005).
6. U. K. Chettiar, A. V. Kildishev, T. A. Klar, and V. M. Shalaev, "Negative index metamaterial combining magnetic resonators with metal films," Opt. Express **14**, 7872–7877 (2006).
7. G. Dolling, M. Wegener, C. M. Soukoulis, and S. Linden, "Negative-index metamaterial at 780 nm wavelength," Opt. Lett. **32**, 53–55 (2007).
8. J. B. Pendry, A. J. Holden, W. J. Stewart, and I. Youngs, "Extremely low frequency plasmons in metallic mesostructures," Phys. Rev. Lett. **76**, 4773–4776 (1996).
9. J. B. Pendry, A. J. Holden, D. J. Robbins, and W. J. Stewart, "Magnetism from conductors and enhanced nonlinear phenomena," IEEE Trans. Microwave Theory Tech. **47**, 2075–2084 (1999).
10. S. Zhang, W. Fan, B. K. Minhas, A. Frauenglass, K. J. Malloy, and S. R. J. Brueck, "Midinfrared resonant magnetic nanostructures exhibiting a negative permeability," Phys. Rev. Lett. **94**, 037402 (2005).
11. A. V. Kildishev, W. Cai, U. K. Chettiar, H.-K. Yuan, A. K. Sarychev, V. P. Drachev, and V. M. Shalaev, "Negative refractive index in optics of metal-dielectric composites," J. Opt. Soc. Am. B **23**, 423–433 (2006).
12. J. L. Volakis, A. Chatterjee, and L. C. Kempel, *Finite Element Method for Electromagnetics* (IEEE Press, Piscataway, NJ, 1998).
13. D. R. Smith, S. Schultz, P. Markoš, and C. M. Soukoulis, "Determination of effective permittivity and permeability of metamaterials from reflection and transmission coefficients," Phys. Rev. B **65**, 195104 (2002).
14. V. A. Podolskiy, A. K. Sarychev, and V. M. Shalaev, "Plasmon modes in metal nanowires and left-handed materials," J. Nonlinear Opt. Phys. Mater. **11**, 65–74 (2002).
15. G. Shvets and Y. A. Urzhumov, "Negative index meta-materials based on two-dimensional metallic structures," J. Opt. A – Pure Appl. Op. **8**, S122–S130 (2006).
16. P. B. Johnson and R. W. Christy, "Optical constants of the noble metals," Phys. Rev. B **6**, 4370–4379 (1972).

#78208 - $15.00 USD Received 18 December 2006; revised 25 January 2007; accepted 28 January 2007

1. Introduction

Since the first successful demonstration of a material engineered to have a negative refractive index in the microwave regime [1], interest in negative index metamaterials (NIMs) has experienced an explosive growth. This is primarily due to the predictions for a variety of novel NIM applications (including flat optics and the "perfect lens" [2]), which could not be realized using conventional positive index materials. More recently, a considerable amount of effort has gone into investigating ways to develop NIM realizations that target infrared (IR) and even visible wavelength applications. For example, NIM realizations have been reported that operate in the near-infrared (near-IR) [3, 4, 5, 6] and visible spectrum [7].

In most NIM realizations to date, negative permittivities have been obtained by the Lorentz-Drude behavior of the dielectric functions of noble metals in their native form [3, 6] or by introducing thin-wire structures to achieve lower frequency equivalents [8]. In contrast, magnetic resonance phenomena have been employed exclusively to realize negative permeabilities. For example, circular split-ring resonators have been introduced for application in the microwave range [9]. More recently simpler planar resonator structures have been devised for higher frequencies [4, 5, 7, 10, 11], which are amenable to nano-fabrication technologies.

Up to this point, all NIMs reported in the literature have been designed to exhibit single-band negative index behavior. This paper reports the first numerical validation of dual-band NIM performance in the near-IR achieved by embedding magnetic resonators of two different sizes within the unit cell of a singly- or doubly-periodic metamaterial structure. NIMs are known to be dispersive and consequently a narrowband operating condition is required. Hence, our dual-band NIM designs represent a first step towards expanding their functionality to multi-band regimes. A finite-element boundary-integral analysis method [12] with periodic boundary conditions has been employed to obtain the simulation results presented in this study. Transmission and reflection coefficients obtained from the full-wave electromagnetic analysis were converted to effective parameters of a homogenized layer via well-established inversion procedures [11, 13].

2. Dual-band magnetic resonator

A pair of noble metal nanorods [11, 14] or their two dimensional equivalents [6, 15] have been shown to exhibit negative permeability associated with a magnetic resonance phenomenon. An additional magnetic resonance can be introduced at a different wavelength by including a second resonator structure in the metamaterial design. Figure 1(a) shows one period of a two-dimensional metamaterial structure that exhibits a dual-band magnetic resonance property. Figure 1(b) contains plots that show how the real part μ' of the effective permeability $\mu = \mu' + i\mu''$ is influenced by the length w_2 of the second magnetic resonator. The magnetic resonator comprises a thin layer of alumina between two strips of silver. The space between the magnetic resonators is filled with silica (SiO_2). A protective thin layer of silica with thickness t_s is also placed on the top side of the magnetic resonators with a matching silica layer used on the bottom side to maintain symmetry. The NIM structure is then placed on top of a thick layer of glass, which is treated as a half-space in the analysis. The thick glass layer is not considered to be silica in its purest form, since it is representative of glass supporters that may be used in a laboratory environment on which the metamaterials under test would be mounted for characterization of their optical properties. Finally, the structure is illuminated by a monochromatic plane wave with an $\hat{x}$-directed electric field at normal incidence.

Alumina, silica, and glass are treated as homogeneous, isotropic dielectric materials with indices of refraction equal to 1.62, 1.445, and 1.5, respectively. Experimental results for the dielectric function by Johnson and Christy [16] are used to represent the bulk silver property. The fixed geometrical parameters in Fig. 1(a) are given by $p = 1200$ nm, $w_1 = 300$ nm, $t =$

#78208 - $15.00 USD Received 18 December 2006; revised 25 January 2007; accepted 28 January 2007

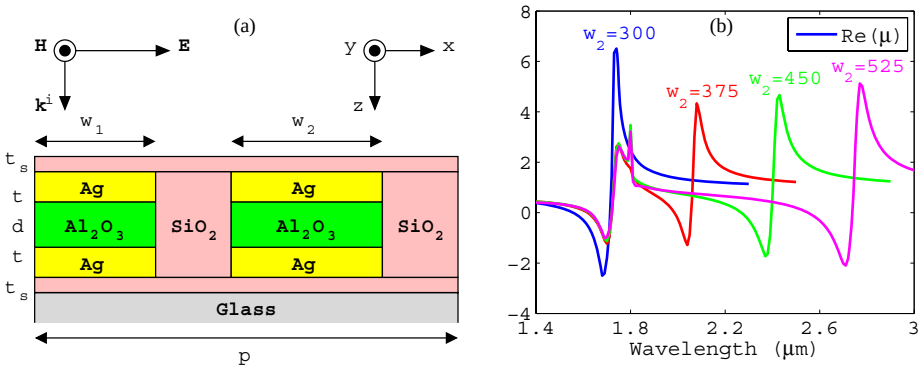

Fig. 1. A dual-band magnetic resonator: (a) Unit cell geometry. (b) Real part of its effective permeability for the designs with $p = 1200$ nm, $w_1 = 300$ nm, $t = 30$ nm, $d = 40$ nm, and $t_s = 20$ nm.

30 nm, $d = 40$ nm, and $t_s = 20$ nm.

Figure 1(b) shows that a second magnetic resonator introduces a strong second resonance where the corresponding wavelength strongly correlates with w_2. The maximum negative permeability achieved by these second resonances becomes stronger as the length w_2 is increased. The first magnetic resonance is weaker than in the corresponding single resonator case ($w_2 = 300$ nm), however the value of μ' at the second resonance becomes negative in every case.

3. Two-dimensional dual-band NIM

Negative permittivity, as required for negative index behavior, can be supplied by the negative bulk permittivity of metals as has been demonstrated for the single-band NIM design presented in [6]. Figure 2 shows a dual-band NIM geometry as well as the effective index of refraction $n = n' + in''$, the effective permittivity $\varepsilon = \varepsilon' + i\varepsilon''$, and the effective permeability $\mu = \mu' + i\mu''$ for $t_f = 6$ nm. All other dimensions are the same as for the magnetic resonator shown in Fig. 1. Dual-band negative index behavior can be observed in Fig. 2(b) for all three geometries with $w_2 > 300$ nm. In addition, the negative values of n' at the second resonance becomes more pronounced as w_2 is increased. Minimum loss, represented by n'', over the second resonance wavelengths is actually lower for larger values of w_2 due to the associated stronger magnetic resonances shown in Fig. 2(d). Due to higher loss of the bulk silver at longer wavelengths, μ' never reaches negative values for the second resonances in contrast to the negative values attained for the magnetic resonator geometries as shown in Fig. 1(b). However at shorter wavelengths, negative values of μ' are obtained resulting in $n'' \approx 1$ around wavelengths corresponding to the first resonance.

As previously discussed, the negative permeability of the bulk metamaterial is realized by magnetic resonances. On the other hand, however, the effective negative permittivity is obtained from the negative permittivities of metals at near-IR wavelengths arising from plasmons. When the negative permittivity effect of silver, comprising both the magnetic resonators and the metal films, outweighs the net positive permittivities of other constituent materials in an averaging fashion, the total structure will possess an effective negative permittivity. This averaging effect can be seen in Fig. 2(c), where ε' for the case in which $w_2 = 525$ nm has the lowest overall value. Therefore, the thickness t_f of the metal films has a direct impact especially on ε and consequently on n. The performance of three dual-band geometries with different values of t_f corresponding to 6, 10, and 20 nm are analyzed in Fig. 3 for the designs with $w_2 = 525$ nm. The range of negative n' moves towards shorter wavelengths with increasing t_f. More importantly,

#78208 - $15.00 USD Received 18 December 2006; revised 25 January 2007; accepted 28 January 2007

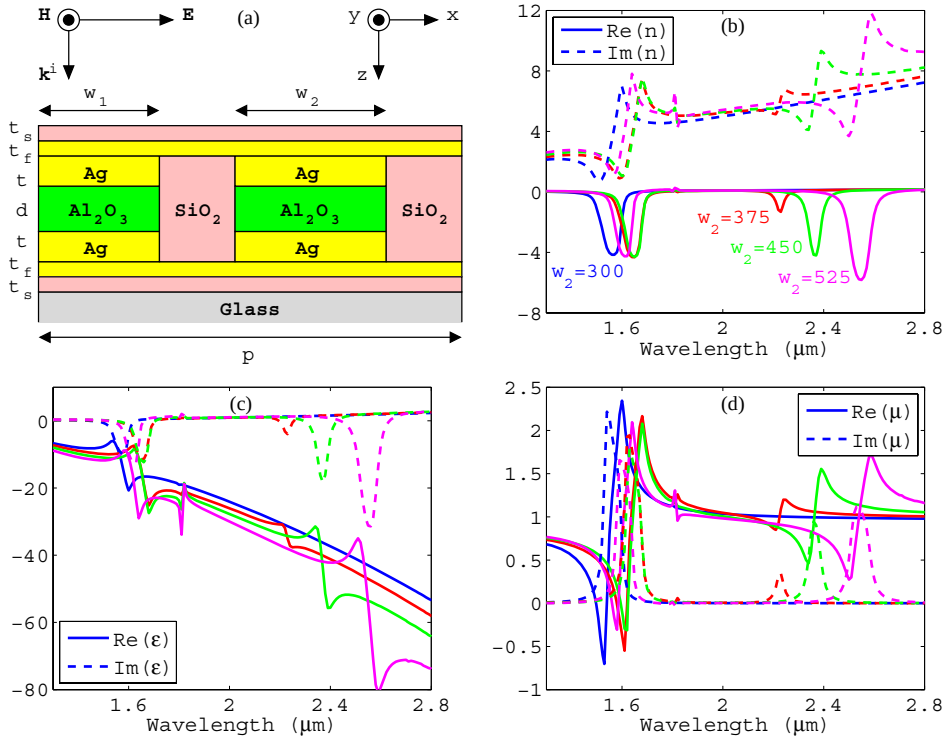

Fig. 2. A two-dimensional dual-band NIM: (a) Unit cell geometry, (b) n, (c) ε, and (d) μ. Two silver films of thickness t_f are added to the magnetic resonator geometry in Fig. 1(a), bounding the resonators from the $\pm\hat{z}$ directions.

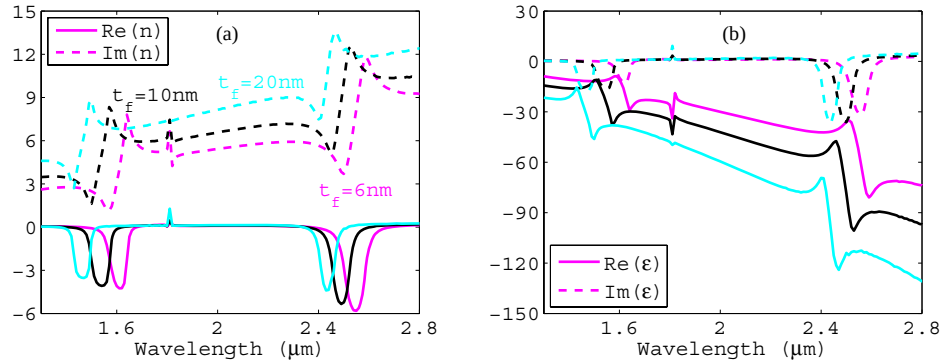

Fig. 3. Effect of silver layer thickness t_f on (a) n and (b) ε for the designs with $w_2 = 525$ nm.

one can note from Fig. 3(a) that n'' increases roughly linearly with t_f, which may be related to the exponential decay of fields in the $+\hat{z}$ direction as they propagate through the silver films. A strong dependence of ε on t_f can be observed in Fig. 3(b).

Although the design with $t_f = 6$ nm is preferred because of its low loss characteristics, it is not practical since silver does not form a continuous metallic layer at such a small thickness. A thickness of 20 nm is considered to be the minimum value at which silver will form a continuous layer [6], but for this value the performance in terms of losses of the NIM will degrade significantly. More precisely, for $t_f = 20$ nm, a value of $n = -1.56 + i7.48$ corresponding to $\lambda = 2.40$ μm was found to exhibit the lowest loss within the second negative-index band,

#78208 - $15.00 USD Received 18 December 2006; revised 25 January 2007; accepted 28 January 2007

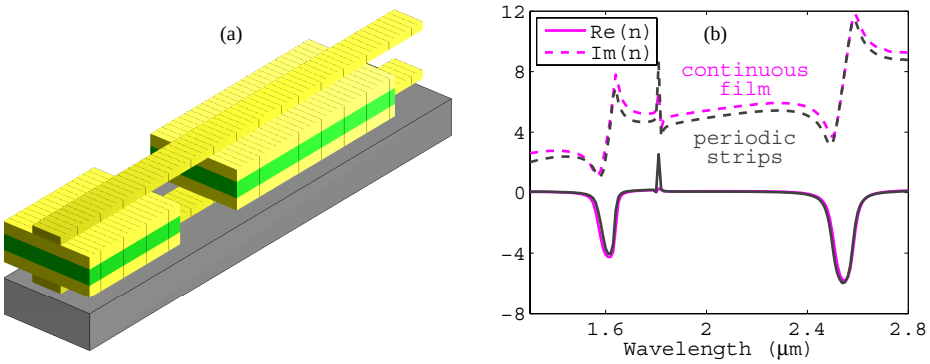

Fig. 4. A dual-band NIM geometry with periodic metal strips providing negative permittivity: (a) Unit cell geometry, (b) Comparison of n for the designs with $w_2 = 525$ nm. For visualization, the volume occupied by silica is shown transparent. The performance of the two-dimensional design in Fig. 2(a) with $t_f = 6$ nm is used for comparison. The periodic silver strips have $t_f = 20$ nm, width of 80 nm, and period of 240 nm.

whereas the best figure for $t_f = 6$ nm was found to be $n = -2.77 + i3.69$ at $\lambda = 2.50\,\mu$m, which has a significantly smaller value of n''.

This trade-off problem between the loss characteristic and fabrication difficulty can be solved by introducing discontinuities in the $\pm\hat{y}$ directions for the silver films. Rather than requiring a continuous metallic layer, thicker metal strips that are infinite in the $\pm\hat{x}$ directions can be placed periodically along the $\pm\hat{y}$ directions. One possible realization is illustrated in Fig. 4(a), where silver strips of thickness 20 nm and width 80 nm provide negative permittivity instead of using continuous silver films. Use of periodic strips in place of continuous films dramatically improves the loss characteristics. The smallest n'' over the second negative-index band is reduced from 7.48 in the case of the continuous films down to 3.14 for periodic strips of the same thickness $t_f = 20$ nm. The effective index of refraction is actually comparable to that of the two-dimensional thin film structure with $t_f = 6$ nm as shown in Fig. 4(b). Moreover, the two curves for n' practically fall on top of each other. The value of n'' for the design with the periodic strips is almost the same but slightly lower than it is for the design that uses the 6 nm-thick continuous films. Therefore, the introduction of periodic metal strips for achieving negative permittivity improves loss characteristics while at the same time ensuring proper silver thickness for fabrication.

4. Doubly-periodic dual-band NIM

The dual-band NIMs shown in Figs. 2(a) and 4(a) provide negative-index behavior for one polarization, namely when the incident electric field is $\hat{x}$-directed. Polarization-independent dual-band NIM behavior can be obtained by a direct extension of these two-dimensional geometries to their three-dimensional counterparts. Figure 5 shows such an example, where magnetic resonances at two distinct wavelength ranges are provided by resonators made of square nano-plates separated by a thin alumina layer. The two magnetic resonators are placed in an alternating order in the four quadrants of a unit cell as illustrated in Fig. 5(a). Negative permittivities are provided by the thin silver mesh structure located on both sides of the magnetic resonators. As before, the doubly periodic three-dimensional NIM design is placed on a thick glass substrate.

In this example, the periods along the $\hat{x}$ and the $\hat{y}$ directions are assumed to be the same with $p = 1200$ nm. Dimensions of the two magnetic resonators in the $x-y$ plane are given by 450 nm $\times$ 450 nm and 375 nm $\times$ 375 nm, respectively. Their dimensions in the $\hat{z}$ direction are the same as for the two-dimensional design illustrated in Fig. 2(a). Also, the cross-sectional

#78208 - $15.00 USD Received 18 December 2006; revised 25 January 2007; accepted 28 January 2007

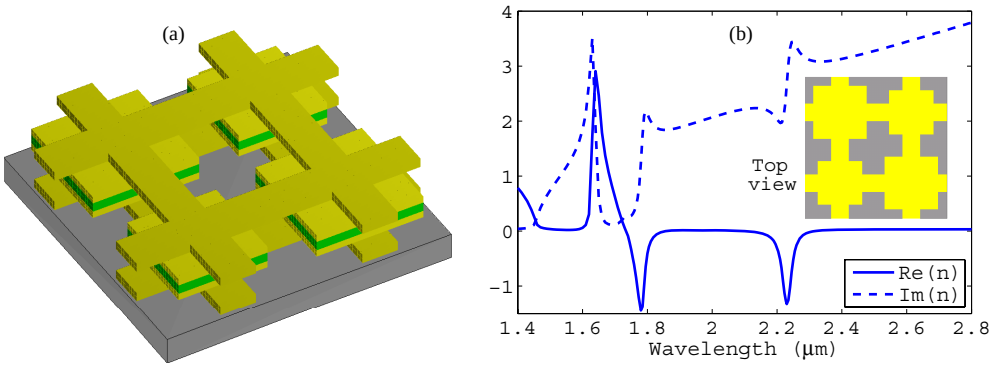

Fig. 5. A doubly-periodic polarization-independent dual-band NIM design: (a) Unit cell geometry, (b) Index of refraction n. The volume occupied by silica is again shown transparent, including the 20 nm-thick layers bounding the electric and the magnetic structures from both sides.

dimensions of the silver mesh were chosen as 150 nm $\times$ 40 nm.

Figure 5(b) shows that two negative-index bands exist for this design around $\lambda = 1.78\ \mu$m (with $n' \approx -1.4$) and $\lambda = 2.23\ \mu$m (with $n' \approx -1.3$). In addition, the inset shows the top view of the polarization-independent design, from which differences in the two magnetic resonator geometries can be compared. The trend in the imaginary part of the effective refractive index n'' is generally seen to increase with wavelength, primarily because of the increasingly larger loss in silver at longer wavelengths. A useful quality measure q of a negative-index band is given by $q = -n'/n''$. Based on this definition, the best quality measures in the two negative index bands for this design were found to be $q = 1.77$ with $n = -0.65 + i0.37$ at $\lambda = 1.76\ \mu$m and $q = 0.50$ with $n = -1.33 + i2.66$ at $\lambda = 2.23\ \mu$m, respectively.

5. Conclusion

Near-infrared metamaterial designs that exhibit dual-band negative-index properties have been presented. For two-dimensional structures, continuous layers of silver were used to provide negative permittivity. The magnetic resonances at two distinct wavelengths were provided by two sets of silver nano-strip pairs with different widths. Results of numerical simulations confirm the dual-band negative-index characteristics of these metamaterials.

The design methodology for a doubly-periodic polarization-independent dual-band NIM structure was introduced. Two pairs of square nano-plates made of silver (each pair a different size) are used to provide magnetic resonances in two distinct bands. A silver mesh provides the negative permittivity without incurring the high losses that would be expected from continuous silver sheets.

We also demonstrated some means of controlling the effective optical constants in the proposed designs. This is of significant importance in super-resolution applications, where it would be necessary to balance losses and impedance of the metamaterial at both operation bands. Specific design parameter values can be adjusted with respect to the quality measure to arrive at the best-performing design. This optimization problem is a subject of current investigation.

Acknowledgments

The authors would like to thank the anonymous reviewer for providing helpful suggestions. This work was supported in part by the Penn State Materials Research Institute and the Penn State MRSEC under NSF grant DMR 0213623, and also in part by ARO grant W911NF-04-1-0350, NSF-PREM grant #DMR-0611430, and by ARO-MURI award 50342-PH-MUR.

#78208 - $15.00 USD Received 18 December 2006; revised 25 January 2007; accepted 28 January 2007